

## Reaction $K^- + n \rightarrow \Lambda^0 + \pi^-$ from 1550 to 1650 MeV\*

W. A. Morris, J. R. Albright, A. P. Colleraine,<sup>†</sup> J. D. Kimel, and J. E. Lannutti

Florida State University, Tallahassee, Florida 32306

(Received 9 March 1977)

This paper presents the results of a study of the reaction  $K^- d \rightarrow (p_s) \Lambda^0 \pi^-$ . The cross section for the process  $K^- n \rightarrow \Lambda^0 \pi^-$  has been measured as a function of the center-of-mass energy in the range from 1550 to 1650 MeV. An energy-dependent partial-wave analysis was performed for this reaction, and two acceptable solutions were found. The first solution indicated no resonant structure in this energy range below the  $\Sigma(1670)$ . The second solution indicated resonant structure in the  $S_{11}$  partial wave with  $E_R = 1600 \pm 6$  MeV/ $c^2$ ,  $\Gamma(E_R) = 87 \pm 19$  MeV/ $c^2$ , and  $x = 0.12 \pm 0.02$ .

### INTRODUCTION

This paper represents the results of a study of the reaction

$$K^- + n \rightarrow \Lambda^0 + \pi^-$$

in the center-of-mass energy range from 1550 to 1650 MeV. Data were collected at two separate beam momenta with the Fermi motion of the nucleons giving a continuous spread in c.m. energy.

In this energy region a number of possible resonances have been reported. Evidence for a possible resonance strongly coupled to the  $\Lambda\pi$  final state has been found by Crennell *et al.*<sup>1</sup> in a production experiment and in the multichannel analyses of Kim<sup>2</sup> and Langbein and Wagner.<sup>3</sup> All three placed this  $S = -1$ ,  $I = 1$  resonance at approximately 1620 MeV, and the multichannel analyses both assigned  $\frac{1}{2}^-$  as the spin-parity of this state. Possible resonant structure at 1583 MeV has been seen by Litchfield<sup>4</sup> and by Carroll *et al.*<sup>5</sup> with an assignment of  $\frac{3}{2}^-$  for the spin-parity by Litchfield. In addition, Carroll *et al.* observed resonant structure at 1608 and 1633 MeV; the three resonances reported by Carroll *et al.* all have widths less than or equal to 15 MeV. The multichannel analyses obtained a width of approximately 50 MeV for the  $\Sigma(1620)$ .

There have been a number of experiments which failed to see any resonant structure in this range. The neutral- $K$ -meson experiments of Cho *et al.*<sup>6</sup> and Bertanza *et al.*<sup>7</sup> both have no evidence for any resonant structure below the well established  $\Sigma(1670)$  in this region. Also the analysis of deBellefon and Berthon<sup>8</sup> fails to require a resonance below 1670 MeV.

This experiment was undertaken in hopes of shedding some light on resonant structure below the  $D_{13}$  at 1670 MeV. The final state of interest is pure  $I = 1$ ; the charged beam and distinct primary

vertex help reduce the uncertainty in kinematic variables; and the Fermi motion within the target yields a continuous energy range to study.

### DATA ACQUISITION

The data for this experiment came from a 120000-picture exposure of the Columbia-Brookhaven 30-inch deuterium-filled bubble chamber at the Alternating Gradient Synchrotron to a low-energy separated  $K^-$  beam.<sup>9</sup> The exposure was divided into two parts corresponding to  $K^-$  momenta at the center of the chamber equal to 630 and 578 MeV/ $c$ ; Fig. 1 is a histogram of the beam momentum obtained from a sample of  $\tau$  decays. The lower momentum was obtained by placing an inch thickness of copper plate in the

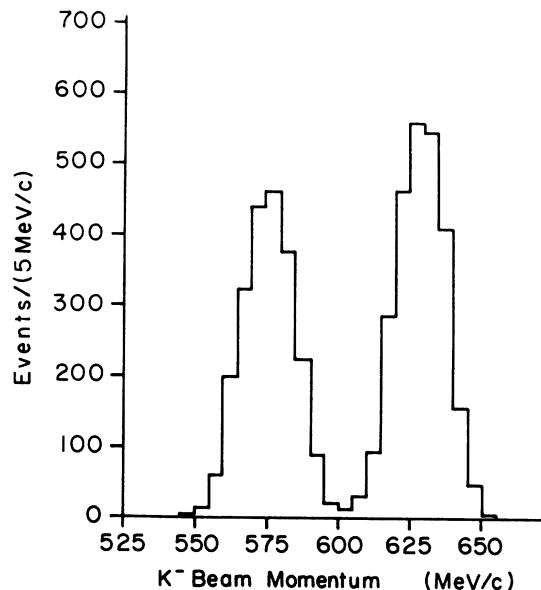


FIG. 1. Beam momentum from  $\tau$  decays.

beam path at the entrance to the bubble chamber to degrade the higher momentum.

All the film was double-scanned to determine scanning efficiencies. The film was scanned for the following topologies:

- (1) three-prong events,
- (2) two-prong-plus-vee events where the positive track at the primary vertex stopped inside the bubble chamber.

To ensure a high scan efficiency and to minimize possible reconstruction problems, a restricted fiducial volume was imposed. This enabled us to obtain a scan efficiency for the three-prong events of 98% and for the two-prong-plus-vee events of 95%. Measurements of all events were made on film-plane or image-plane devices and processed through local versions of the geometry and kinematics programs TVGP and SQUAW. Events which failed to pass the geometry program or which failed to give at least one fit in the kinematic program with a confidence level greater than 1% were remeasured once; events still unresolved were inspected at a scan table to be sure there was no bias being introduced by excluding them from the data sample.

The average beam momentum at each setting was determined from four-constraint kinematic fits to  $\tau$  decays. The  $K^-$  path length was calculated from the number of successfully fitted  $\tau$  decays corrected for scanning and kinematic reconstruction losses. The microbarn equivalence can be expressed as follows:

$$\begin{aligned} \text{No. of events}/\mu\text{b} &= (\text{No. of } \tau \text{ decays}) \\ &\times p_{K^-} \times 5.12 \times 10^{-4} \quad (\text{Ref. 10}), \end{aligned}$$

where  $p_{K^-}$  is the  $K^-$  beam momentum in GeV/c. At 630 MeV/c (578 MeV/c) the corrected number of  $\tau$  decays was  $3349 \pm 70$  ( $3206 \pm 46$ ), which gives a microbarn equivalence of  $1.079 \pm 0.22$  ( $0.943 \pm 0.014$ ) events/ $\mu\text{b}$ .

For the second class of events, the two-prong vees, for those which did not give a three-constraint fit to the decay,  $\Lambda^0 \rightarrow \pi^- p$ , no attempt was made to do a multivertex fit. For the events which had an acceptable  $\Lambda^0$  decay fit, an attempt was made to fit to the following reactions:

- (a)  $K^- d \rightarrow (p_s) \Lambda^0 \pi^-$ ,  $\Lambda^0 \rightarrow \pi^- p$ ,
- (b)  $K^- d \rightarrow (p_s) \Lambda^0 \pi^- \pi^0$ ,  $\Lambda^0 \rightarrow \pi^- p$ ,
- (c)  $K^- d \rightarrow (p_s) \Sigma^0 \pi^-$ ,  $\Sigma^0 \rightarrow \Lambda^0 \gamma$ ,  $\Lambda^0 \rightarrow \pi^- p$ .

An acceptable fit to any of these three reactions was initially defined as one which had a confidence level greater than 1%; 2816 events gave an acceptable fit to one or more of these reactions. To

resolve the ambiguous events, numbering 486, the confidence levels for the fits were used in the following manner. If only one fit had a confidence level above 5% or the highest confidence level was more than three times the next highest, this one fit or this highest-confidence-level fit was taken as the correct fit; this resolved most of the ambiguities involving a  $\Lambda^0 \pi^-$  fit. Of the approximately 50 remaining events involving  $\Lambda^0 \pi^- - \Sigma^0 \pi^-$  ambiguities, if the cosine of the angle between the direction of the  $\gamma$  in the  $\Sigma^0$  c.m. system and the direction of the  $\Sigma^0$  was less than  $-0.85$ , the event was accepted as a  $\Lambda^0 \pi^-$  fit; otherwise the event was classed as a  $\Sigma^0 \pi^-$  fit. The value  $-0.85$  was chosen because in a study of this cosine of the angle for the few ambiguous events, there was a slight deviation from the expected isotropy below  $-0.85$  which can be caused by  $\Lambda^0$  events being misfitted as  $\Sigma^0$  events. While an absolute cut as used would class some  $\Sigma^0$  events as  $\Lambda^0$  events, it was estimated that only six events would so be mislabeled. Using these criteria we assigned 216 of the 486 ambiguous events to the  $\Lambda^0 \pi^-$  channel; this gave a total of 1613  $K^- d \rightarrow (p_s) \Lambda^0 \pi^-$  events.

#### BIAS CORRECTIONS

In scanning for events which might fit to  $K^- d \rightarrow (p_s) \Lambda^0 \pi^-$ , we required the event to have a visible stopping spectator proton and a visible  $\Lambda^0$  decay. Thus we can divide our bias corrections into those involving the spectator proton and those involving the  $\Lambda^0$  decay. Figure 2 is a histogram of the momenta of the spectator protons; the lower curve is the predicted shape for the spectator momentum distribution from the Hulthén wave function<sup>11</sup> assuming a minimum projected length for the proton of 1.25 mm; the upper curve is the prediction for zero minimum projected length. Both curves were normalized to the data between 100 and 250 MeV/c. We then excluded events for which the spectator protons had a minimum projected length less than 1.25 mm; to minimize the effects of double scattering we also excluded events with spectator momenta greater than 280 MeV/c. The ratio of the area under the upper curve to that under the lower curve was used to correct for unseen spectator protons, and the reciprocal of the fraction of the area under the curve below 280 MeV/c was used to correct for the fast-spectator cut in the cross-section calculations.

Since the  $\Lambda^0$  decays visibly to  $\pi^- p$  only 64.2% of the time,<sup>12</sup> the major correction for undetected  $\Lambda^0$  decays was one over the branching fraction. Also, because of a scanning bias against short  $\Lambda^0$  decay lengths, a minimum length of 3 mm was required for the  $\Lambda^0$ , and the decay had to occur within a

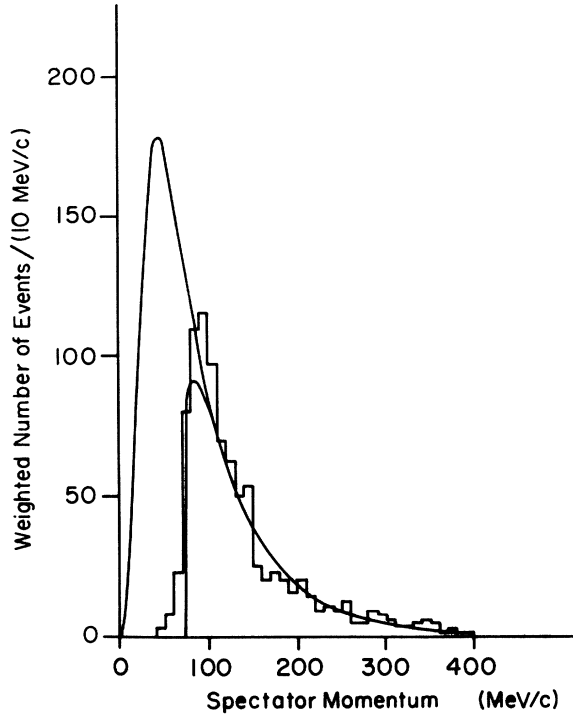


FIG. 2. Spectator momentum. The curves represent the predictions of the Hulthén wave function for a 1.25-mm minimum length (lower curve) and for zero minimum length (upper curve) cut on the spectator proton.

cylinder of a 30-cm radius with ends at  $Z=0.0$  and  $Z=-30.0$  cm in the bubble-chamber coordinate system. When the length of the  $\Lambda^0$  was studied, the loss in events was only significant when the length was less than 2 mm; however, the more conservative 3 mm was used to guard against different sensitivities for different scanners. To correct for these cuts, each event was weighted by the reciprocal of the probability of decay in the fiducial volume thus defined.

Losses of  $\Lambda^0$ 's due to short tracks of decay products were corrected for by imposing a minimum projected length cut of 1.25 mm, corresponding to cuts in the  $\cos\delta$  distribution, where  $\delta$  is the angle between the decay product track in the rest frame of the  $\Lambda^0$  and the direction of the  $\Lambda^0$ . A weight,

$$W = 2/(1 - \cos\delta_c),$$

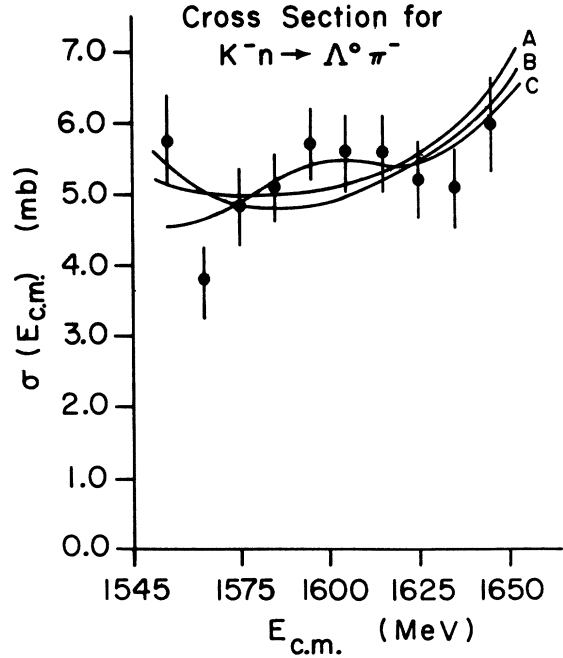


FIG. 3. Channel cross section for  $K^-n \rightarrow \Lambda^0\pi^-$  as a function of the center-of-mass energy. The three curves correspond to different solutions for the partial wave fittings, as discussed in the text.

was applied to the remaining events where  $\delta_c$  is the value of  $\delta$  corresponding to the length cutoff for the decay product tracks for a  $\Lambda^0$  of the measured momentum.

Since there were no discernable losses of  $\Lambda^0$ 's whose decay planes were parallel to the optical axis, no corrections were made. Corrections were made for scanning efficiency, unmeasured events, geometry and kinematic program failures, and for the 1% probability cut.

Finally, because of the presence of two nucleons in deuterium, the single nucleon cross sections must be corrected for a screening effect.<sup>13</sup> We defined this correction factor by

$$W = \left( 1 - \frac{\sigma_{\text{tot}}(K^-p)}{4\pi} \left\langle \frac{1}{r^2} \right\rangle \right)^{-1},$$

where  $\langle 1/r^2 \rangle = 0.0423 \text{ mb}^{-1}$ , and where the  $K^-p$  cross sections were taken from Carroll *et al.*<sup>5</sup>

Table I gives the number of events before cuts were made, the number of unweighted events after

TABLE I. Channel cross sections.

Momentum	No. of events before cuts	No. of events after cuts	Weighted No. of events	$\sigma(K^-d \rightarrow (p_s)\Lambda^0\pi^-)$
630 MeV/c	914	802	$6130 \pm 216$	$5.68 \pm 0.20 \text{ mb}$
578 MeV/c	699	614	$5440 \pm 207$	$5.77 \pm 0.22 \text{ mb}$

the cuts were made, and the cross sections for the reaction  $K^-d \rightarrow (p_s) \Lambda^0 \pi^-$  at the two beam momentum values. In order to get the cross section as a function of c.m. energy, the beam momentum distribution and the Hulthén wave function were used to calculate the fraction of events expected in the c.m. energy interval  $E - \Delta E$  to  $E + \Delta E$  assuming a constant cross section. The events were binned in identical energy intervals and weighted by the reciprocal of the fraction expected for that interval. Figure 3 is a plot of  $\sigma(K^-n \rightarrow \Lambda^0 \pi^-)$  versus c.m. energy; the curves shown in Fig. 3 are results from the partial-wave fitting and will be explained below.

#### PARTIAL-WAVE ANALYSIS

For the energy-dependent partial-wave analysis of these data, we chose to express the differential cross sections in terms of helicity amplitudes. Thus we write

$$\frac{d\sigma}{d\Omega} = |f_{(1/2)(1/2)}(\theta)|^2 + |f_{(1/2)(-1/2)}(\theta)|^2,$$

where

$$f_{\lambda' \lambda}(\theta) = \frac{1}{p} \sum_J (2J+1) T_{\lambda' \lambda}^J d_{\lambda' \lambda}^J(\theta),$$

where  $\lambda$  and  $\lambda'$  are the helicities of the neutron and  $\Lambda$ , respectively,  $d_{\lambda' \lambda}^J(\theta)$  is the reduced rotation function, and  $T_{\lambda' \lambda}^J$  is the partial-wave projection of the transition amplitude between initial and final states.<sup>10</sup> Also the polarization  $P$  is defined as

$$P = \frac{2 \operatorname{Im}[f_{(1/2)(1/2)}(\theta) f_{(1/2)(-1/2)}^*(\theta)]}{[|f_{(1/2)(1/2)}(\theta)|^2 + |f_{(1/2)(-1/2)}(\theta)|^2]}.$$

The data were divided into five energy intervals and each energy interval was subdivided into 10  $\cos\theta$  intervals. For each of these 50 bins, the average polarization of the  $\Lambda^0$  was calculated from

$$\frac{1}{3} \alpha P = \langle \cos\eta \rangle,$$

where  $\alpha = 0.647$  is the  $\Lambda^0$  decay asymmetry parameter<sup>14</sup> and the angle  $\eta$  is defined by

$$\cos\eta = \hat{P}_\Lambda \cdot (\hat{K} \times \hat{\Lambda}),$$

where  $\hat{K}$  and  $\hat{\Lambda}$  are unit vectors in the direction of the  $K^-$  and  $\Lambda^0$ , respectively, in the overall center-of-mass system, and  $\hat{P}_\Lambda$  is a unit vector in the direction of the proton from the  $\Lambda^0$  decay in the  $\Lambda^0$  center-of-mass system.

The transition amplitudes for the background terms were parametrized as

$$T_B = a + b p_K,$$

where  $a$  and  $b$  are complex constants and  $p_K$  is the

equivalent incident  $K^-$  momentum in the laboratory system in GeV/ $c$  for the given c.m. energy. The parametrization for the resonant terms was

$$T_R = x/(\epsilon - i),$$

where  $\epsilon = 2(E_R - E)/\Gamma$  and  $x = \pm(\Gamma_e \Gamma_r/\Gamma^2)^{1/2}$ , where  $E$  is the c.m. energy,  $E_R$  is the mass of the resonance,  $\Gamma_e$  is the elastic channel partial width,  $\Gamma_r$  is the reaction channel partial width, and  $\Gamma = \sum_i \Gamma_i$ , where the summation is over all decay channels of the resonance. To approximate the energy dependence of  $\Gamma$  we used the relation

$$\Gamma(E) = \Gamma(E_R)(k/k_R)^{2l+1},$$

where  $k$  is the momentum of the outgoing particle in the overall center-of-mass system and  $k_R$  is the value at  $E = E_R$ . The fitting was done to the parameters  $a$ ,  $b$ ,  $x$ ,  $\Gamma$ , and  $E_R$  with the following restrictions and assumptions:

(a) The mass of any resonance had to lie between 1550 and 1650 MeV/ $c^2$ .

(b) The width of the resonance had to lie between 10 and 150 MeV/ $c^2$ .

(c) Only waves up to  $D_{15}$  were included.

(d) The  $D_{13}$  and  $D_{15}$  were fixed as being resonant waves with mass and width fixed for both waves and the amplitude for the  $D_{15}$  also fixed.

(e) Unitarity was imposed on the amplitudes.

(f) A particular partial wave was assumed to be either resonant or background but not both.

This last assumption was checked by letting the partial-wave amplitude be described by

$$T = T_R + T_B,$$

and seeing whether it improved the fits significantly. The fitting was done by minimizing the  $\chi^2$  given by

$$\chi^2 = \sum_{i=1}^5 \sum_{j=1}^{10} \left[ \left( \frac{d\sigma_{ij}^e/d\Omega - d\sigma_{ij}^p/d\Omega}{\delta(d\sigma_{ij}^e/d\Omega)} \right)^2 + \left( \frac{P_{ij}^e - P_{ij}^p}{\delta P_{ij}^e} \right)^2 \right],$$

where the superscript  $e$  denotes the experimentally measured value and the superscript  $p$  denotes the predicted value from the parametrization. The minimization was done using the FORTRAN subroutine STEPIT.<sup>15</sup> As a check on the results of the fit, the parameters were used to calculate the  $\sigma(K^-n \rightarrow \Lambda^0 \pi^-)$  as a function of energy.

#### RESULTS AND CONCLUSIONS

In order to establish a basis for comparison, a fit was tried with the first three partial waves assumed to be nonresonant and the  $D_{13}$  and the  $D_{15}$  assumed to be resonant. All subsequent solutions

TABLE II. Partial-wave fit parameters,  $S_{11}$  nonresonant.

Nonresonant waves	Re $a$	Im $a$	Re $b$	Im $b$
$S_{11}$	$-0.08 \pm 0.02$	$-0.05 \pm 0.02$	$0.03 \pm 0.02$	$0.01 \pm 0.02$
$P_{11}$	$0.00 \pm 0.02$	$-0.12 \pm 0.02$	$-0.06 \pm 0.02$	$-0.05 \pm 0.02$
$P_{13}$	$-0.20 \pm 0.03$	$-0.03 \pm 0.02$	$0.21 \pm 0.03$	$0.04 \pm 0.02$
Resonant waves	Mass (MeV/ $c^2$ )	Width (MeV/ $c^2$ )	Amplitude at resonance	
$D_{13}$	1670 <sup>a</sup>	50 <sup>a</sup>	$0.13 \pm 0.02$	
$D_{15}$	1765 <sup>a</sup>	120 <sup>a</sup>	$-0.25^a$	

<sup>a</sup> Indicates fixed parameters, not fitted.

were compared to this first fit to find if any significant improvement was made in the quality of the fit as determined by the ratio of the  $\chi^2$  to the number of degrees of freedom. In Fig. 3, the curve labeled A is the predicted cross section as a function of the center-of-mass energy based on the parameters determined in this first fit; the values

of all the fitted parameters are listed in Table II. The  $\chi^2$  per degree of freedom for this fit was 1.76. The only free parameter in the resonant wave was the amplitude at resonance for the  $D_{13}$  wave; our fitted value of  $0.13 \pm 0.02$  is in agreement with the previously measured values.<sup>2,3</sup>

The curve marked B in Fig. 3 is the result for the cross section when the  $P_{11}$  wave was also as-

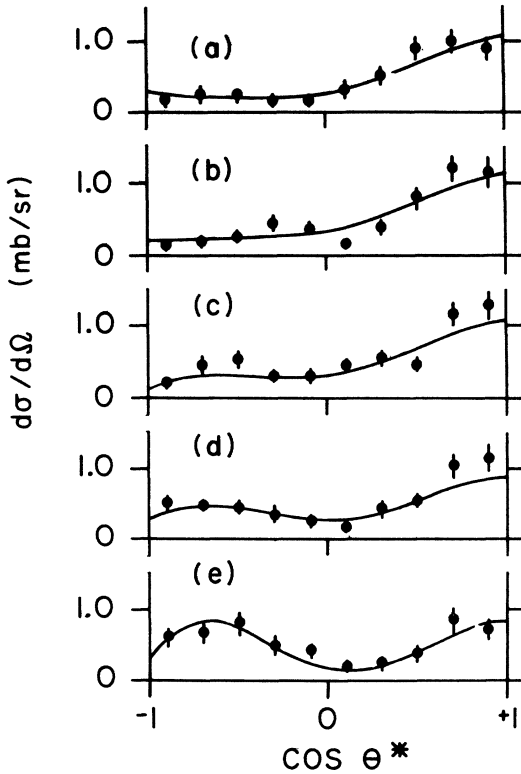


FIG. 4.  $d\sigma/d\Omega$ . The five plots correspond to the five energy intervals: (a) 1550 to 1570 MeV/ $c^2$ , (b) 1570 to 1590 MeV/ $c^2$ , (c) 1590 to 1610 MeV/ $c^2$ , (d) 1610 to 1630 MeV/ $c^2$ , and (e) 1630 to 1650 MeV/ $c^2$ . The curves represent the  $S_{11}$ -resonant solution given in Table III.

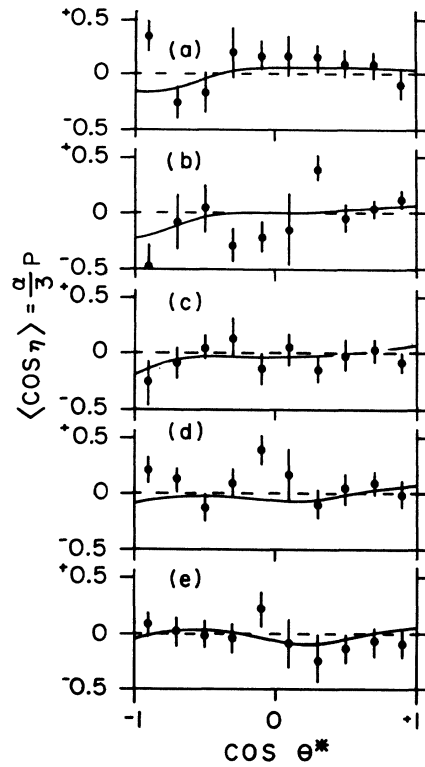


FIG. 5.  $\langle \cos \eta \rangle = \frac{1}{3} \alpha P$ . The five plots correspond to the five energy intervals: (a) 1550 to 1570 MeV/ $c^2$ , (b) 1570 to 1590 MeV/ $c^2$ , (c) 1590 to 1610 MeV/ $c^2$ , (d) 1610 to 1630 MeV/ $c^2$ , and (e) 1630 to 1650 MeV/ $c^2$ . The curves represent the  $S_{11}$ -resonant solution given in Table III.

TABLE III. Partial-wave fit parameters,  $S_{11}$  resonant.

Nonresonant waves	Re $a$	Im $a$	Re $b$	Im $b$
$P_{11}$	$-0.25 \pm 0.03$	$0.43 \pm 0.04$	$0.33 \pm 0.04$	$-0.60 \pm 0.05$
$P_{13}$	$-0.03 \pm 0.01$	$0.00 \pm 0.01$	$0.05 \pm 0.02$	$0.16 \pm 0.02$
Resonant waves	Mass (MeV/ $c^2$ )	Width (MeV/ $c^2$ )	Amplitude at resonance	
$S_{11}$	$1600 \pm 6$	$87 \pm 19$	$0.12 \pm 0.02$	
$D_{13}$	$1670^a$	$50^a$	$0.17 \pm 0.03$	
$D_{15}$	$1765^a$	$120^a$	$-0.25^a$	

<sup>a</sup> Indicates fixed parameters, not fitted.

sumed resonant. The increased upward concavity was found to be characteristic of all fits in which either the  $P$  wave or the  $D$  wave was assumed resonant in this energy region. Also, the fitted parameters tended to take on the limiting values of the mass and width for a resonant wave. Based on the physically unrealistic parameters required by the solutions, on the larger  $\chi^2$ -to-number-of-degrees-of-freedom ratio, and on the obvious inability to reproduce the cross section for this reaction, we must conclude that we have no evidence for resonant behavior in the  $P_{11}$ , or higher partial waves, including the  $D_{13}$  reported at 1583 MeV,<sup>4</sup> in the energy region from 1550 to 1650 MeV.

When the  $S_{11}$  wave was assumed resonant, we obtained the curve labeled C in Fig. 3. Figures 4 and 5 show the data and the results from this fit for  $d\sigma/d\Omega$  and the polarization. Table III lists the parameter values obtained in this fit. The ratio of the  $\chi^2$  to the number of degrees of freedom was 1.80. The parameter values obtained for the  $S_{11}$  resonance were:  $E_R = 1600 \pm 6$  MeV,  $\Gamma = 87 \pm 19$  MeV, and  $x = 0.12 \pm 0.02$ ; for the  $D_{13}$  wave  $x = 0.17 \pm 0.03$ . While Fig. 3 indicates that the  $S_{11}$ -resonant solution reproduces the cross section as a function of c.m. energy better than the  $S_{11}$ -nonresonant solution the  $\chi^2$  per degree of freedom is not significantly different for the two solutions; thus, we feel we must accept both solutions as

possible. The value of the amplitude at resonance for the  $D_{13}$ ,  $x = 0.17 \pm 0.03$ , is larger than normally reported, but such larger values have been frequently found.<sup>3, 16, 17</sup>

The results of the  $S_{11}$ -resonant solution are consistent with previously published work. The analyses of Kim<sup>2</sup> and Langbein and Wagner<sup>3</sup> both require a slightly higher position for the resonance and slightly smaller width. Also, lacking the energy resolution of Carroll *et al.*,<sup>5</sup> we may not be able to distinguish between the narrow resonances they see and the one broad one we see.

In conclusion, we observed two possible solutions for resonant structure in the energy range from 1550 to 1650 MeV. The first requires no resonant behavior in this region; the second suggests the existence of a broad resonance at 1600 MeV with a spin-parity assignment of  $\frac{1}{2}^-$ .

#### ACKNOWLEDGMENTS

The authors would like to thank Professor V. Hagopian and Professor P. K. Williams for informative discussions. We also thank Dr. J. Richy for help with magnetic field problems. We also would like to thank the scanning and measuring staff at the Florida State University for their efforts. We are indebted to the Florida State University Computing Center for their cooperation and support.

\*Work supported in part by the U.S. Energy Research and Development Administration.

†Present address: General Atomics Co., San Diego, California 92138.

<sup>1</sup>D. J. Crennell, W. C. Delaney, E. Flaminio, U. Karshon, K. W. Lai, W. J. Metzger, J. S. O'Neill, J. M. Scarr, A. M. Thorndike, P. Baumel, R. M. Lea, A. Montwill, and T. G. Schumann, Phys. Rev. Lett. **21**, 648 (1968).

<sup>2</sup>J. K. Kim, Phys. Rev. Lett. **27**, 356 (1971).

<sup>3</sup>W. Langbein and F. Wagner, Nucl. Phys. **B47**, 477 (1972).

<sup>4</sup>P. J. Litchfield, Phys. Lett. **51B**, 509 (1974).

<sup>5</sup>A. S. Carroll, I. H. Chaing, T. F. Kycia, K. K. Li, P. O. Mazur, D. N. Michael, P. M. Mockett, D. C. Rahm, and R. Rubinstein, Phys. Rev. Lett. **37**, 806 (1976).

<sup>6</sup>Y. Cho, M. Derrick, D. Lissauer, R. J. Miller, R. P.

- Smith, A. Engler, G. Keyes, R. W. Kraemer, J. Schlereth, and M. Tanaka, Argonne National Laboratory, Report No. ANL-HEP-PR-76-16, 1976 (unpublished).
- <sup>7</sup>L. Bertanza, W. Cameron, P. Capiluppi, P. Croft, E. Flaminio, R. Jennings, C. Kalmus, P. Lugaresi-Serra, G. Mandrioli, A. Minguzzi-Ranzi, W. Morton, A. Nappi, R. Pazzi, K. J. Peach, A. M. Rossi, B. Saita, and W. Venus, Nucl. Phys. B110, 1 (1976).
- <sup>8</sup>A. deBellefon and A. Berthon, Nucl. Phys. B109, 129 (1976).
- <sup>9</sup>D. Berley, Alternating Gradient Synchrotron Division, Technical Report No. 258, 1965 (unpublished).
- <sup>10</sup>W. Morris, Ph. D. dissertation, The Florida State University, 1973 (unpublished).
- <sup>11</sup>L. Hulthén and M. Sugawara, *Handbuch der Physik* (Springer, Berlin, 1957), Vol. 39, pp. 1-143.
- <sup>12</sup>C. Baltay, A. Bridgewater, W. A. Cooper, M. Habibi, and N. Yeh, Phys. Rev. D 4, 670 (1971).
- <sup>13</sup>R. J. Glauber, Phys. Rev. 100, 242 (1955).
- <sup>14</sup>Particle Data Group, Phys. Lett. 50B, 1 (1974).
- <sup>15</sup>J. P. Chandler, Behav. Sci. 14, 81 (1969).
- <sup>16</sup>D. Budgen, Lett. Nuovo Cimento 2, 85 (1971).
- <sup>17</sup>R. A. Ponte, S. S. Hertzbach, J. Button-Shafer, S. S. Yamamoto, E. L. Harte, R. M. Rice, R. B. Bacastow, and S. Y. Fung, Phys. Rev. D 12, 2597 (1975).